Journal of Zhejiang University-SCIENCE A (Applied Physics & Engineering) 2023 24(7):596-611
www.jzus.zju.edu.cn; www.springer.com/journal/11582
E-mail: jzus_a@zju.edu.cn

Research Article

https://doi.org/10.1631/jzus.A2300056

Check for updates

Underwater minirobots actuated by hybrid driving method

Xinghong YE[1,5], Yang YANG[1,3,5], Pengcheng JIAO[1,2✉], Zhiguo HE[1,2,4✉], Lingwei LI[1]

[1]*Institute of Port, Coastal and Offshore Engineering, Ocean College, Zhejiang University, Zhoushan 316021, China*
[2]*Engineering Research Center of Oceanic Sensing Technology and Equipment of Ministry of Education, Zhejiang University, Zhoushan 316021, China*
[3]*Department of Biomedical Engineering (BME), National University of Singapore, Singapore 119077, Singapore*
[4]*Key Laboratory of Marine Geotechnical Engineering and Materials, Zhoushan 316021, China*
[5]*Authors contributed equally to this work*

Abstract: Underwater minirobots have attracted significant interest due to their value in complex application scenarios. Typical underwater minirobots are driven mainly by a soft or rigid actuator. However, soft actuation is currently facing challenges, including inadequate motional control accuracy and the lack of a continuous and steady driving force, while conventional rigid actuation has limited actuation efficiency, environmental adaptability, and motional flexibility, which severely limits the accomplishment of complicated underwater tasks. In this study, we developed underwater minirobots actuated by a hybrid driving method (HDM) that combines combustion-based actuators and propeller thrusters to achieve accurate, fast, and flexible underwater locomotion performance. Underwater experiments were conducted to investigate the kinematic performance of the minirobots with respect to the motion modes of rising, drifting, and hovering. Numerical models were used to investigate the kinematic characteristics of the minirobots, and theoretical models developed to unveil the mechanical principle that governs the driving process. Satisfactory agreement was obtained from comarisons of the experimental, numerical, and theoretical results. Finally, the HDM was compared with selected hybrid driving technologies in terms of acceleration and response time. The comparison showed that the minirobots based on HDM were generally superior in transient actuation ability and reliability.

Key words: Hybrid driving method (HDM); Underwater minirobots; Operation reliability; Transient actuation

1 Introduction

Autonomous underwater vehicles (AUVs) have been developed to carry out various field exploration tasks, e.g., monitoring the health of underwater structures (Neto et al., 2014) and extreme disaster investigation (Sahoo et al., 2019). Such tasks typically require good object pertinence, impressive mobility, and satisfactory control accuracy (Albiez et al., 2015; Dinmohammadi et al., 2019). Recently, AUVs have shown reliable performance in various applications, such as deep-ocean exploration (Iscar et al., 2018), object detection (Song et al., 2021), and maintenance of underwater structures (Sahoo et al., 2019). AUVs are actuated by various methods, such as multi-propeller cooperative propulsion (An et al., 2019), hydraulic propulsion (Zhou et al., 2013), vector propulsion (Chen et al., 2020), and waterjet propulsion (Xin et al., 2013). These actuation methods, however, limit the environmental adaptability and motional flexibility of AUVs (Antonelli et al., 2004). This results in unsatisfactory interactions between the robot systems and previously unmapped marine environments with accidental disturbance, e.g., creature disturbance (Li et al., 2014), fluid disturbance (Yao and Zhao, 2018), and obstacle disturbance (Das et al., 2016).

Inspired by natural creatures, soft robotics and actuators have been developed in recent years to solve the shortcomings of rigid actuators. Unlike conventional rigid components, flexible functional materials undergo compliant and large deformations that provide unique

✉ Pengcheng JIAO, pjiao@zju.edu.cn
Zhiguo HE, hezhiguo@zju.edu.cn
Xinghong YE, https://orcid.org/0000-0003-3298-8108
Yang YANG, https://orcid.org/0000-0002-3899-3752
Pengcheng JIAO, https://orcid.org/0000-0002-9577-3828
Zhiguo HE, https://orcid.org/0000-0002-0612-9062

Received Feb. 1, 2023; Revision accepted Mar. 13, 2023;
Crosschecked May 25, 2023

© Zhejiang University Press 2023

advantages such as flexibility (Li et al., 2018; Zhang et al., 2019), light weight (da Cunha et al., 2020; Zhang et al., 2020), and good environmental interaction (Rus and Tolley, 2015; Lee et al., 2017; Cheng et al., 2018). Based on multifunctional flexible materials, underwater soft actuators can be actuated by various environmental stimuli (Lee et al., 2010; Laschi et al., 2016; Banerjee et al., 2018). A pneumatically powered soft robot with a design based on the pressure response phenomenon, was found to be resilient to a variety of adverse environmental conditions (Tolley et al., 2014b). A biomimetic turtle flipper actuator, actuated by a shape memory alloy (SMA), was developed to perform continuous motions mimicking the forelimb of the green turtle, Chelonia mydas. This design showed better bionic ability than rigid robots (Song et al., 2016). A high-voltage-induced dielectric elastomer (DE) was designed for use in a manta-inspired underwater soft robot that can swim in the Mariana Trench, withstanding the extremely high pressure in the deep sea (Li TF et al., 2017; Li GR et al., 2021). Those studies illustrate the applicability of soft actuators manufactured using flexible functional materials in harsh application scenarios. However, these soft actuators have a limited response time and actuation acceleration. Therefore, improvements in the kinematic performance of soft actuators (i.e., reaction ability and locomotion performance) are needed, while maintaining good maneuverability and environment adaptability.

Using the extreme reaction of combustion (igniting premixed methane and oxygen gas), triple-pedal soft robots with pneu-nets were designed to generate explosive bursts of pressure for on-land high-speed soft robots (Tolley et al., 2014b). A transient driving method (TDM) was proposed to quantitatively study the combustion-based driving method, and the theoretical performance of the TDM-enabled soft actuator was studied (Yang et al., 2020, 2022; He et al., 2023). Untethered underwater soft jumpers were developed to demonstrate the applicability of TDM-based soft robots in a water-air multiphase environment (Wang et al., 2021). The reported soft jumpers were able to leap out of the water by generating powerful thrust to reach an average distance of 2.5 times their body length from the water-air interface and 4.5 times the body length from the initial location, in a time of less than 0.4 s. However, the TDM is currently facing challenges, including inadequate motional control accuracy and the lack of a continuous and steady driving force, and the noise generated by combustion is not conducive to underwater monitoring and other operations.

Here, we report a novel type of underwater minirobot actuated by the hybrid driving method (HDM) that combines conventional driving methods with TDM, i.e., that combines combustion-based actuators with propeller thrusters to achieve accurate, fast, and flexible underwater locomotion performance. This class of robot-hybrids, comprising hard and soft systems functioning synergistically, is capable of performing tasks that neither can do alone. Considering the characteristics of transient velocity movement actuated by combustion and the continuous driving force provided by propeller thrusters, these devices have prospects for application in many underwater scenarios involving minirobots, e.g., underwater transient starting and braking, escaping from being stuck, instantaneous obstacle avoidance, underwater monitoring, and underwater grasping. Table 1 compares aspects of performance of our proposed method with those of similar published methods. To investigate the operational reliability and transient actuation ability, the minirobots were tested in the rising, hovering, and drifting modes. The HDM-based minirobots had a high transient starting velocity of 3–4 m/s. Moreover, the propellers were able to maintain the speed while providing more precise movements. A numerical model based on the dynamic mesh method and a theoretical model based on the drag analysis method were developed, and good agreement was

Table 1 Comparison of the performances of the proposed HDM and similar published driving methods

Reference	Driving method	Response time (ms)	Actuation velocity (BL/s)	Actuation duration
Yang et al., 2020	TDM	~10	~8	0.3 s
Wang et al., 2021	TDM	~10	~9	0.4 s
Kim et al., 2017	Thrusters	~300	~0.6	1–2 h
Zhang et al., 2021	Thrusters	~200	~0.45	1–2 h
Tolley et al., 2014b	HDM	~30	~7.5	0.7 s
This study	HDM	~10	~6	1–2 h

BL is the body length

obtained from a comparison. Parametric comparisons were conducted to demonstrate the effectiveness of the HDM in controlling the locomotion of the minirobots. Finally, the HDM underwater minirobots were compared with existing soft robots driven by different technologies, e.g., shape memory polymers (SMP), magnets, electromagnets (EM), gels, thrusters, and combustion, in terms of their response time and actuation acceleration. The rest of this paper is organized as follows: Section 2 presents the design principle and fabrication process of the underwater minirobots. Section 3 presents the experimental study to investigate the kinematic characteristics of the minirobots. Section 4 develops the numerical and theoretical models to explain the physical principles of the motion process. Section 5 compares and discusses the experimental, numerical, and theoretical results. Section 6 presents the limitations of this study and proposes future work. Section 7 concludes the main findings of this study. The electronic supplementary materials (ESM) provide further details on the experimental performance of the underwater minirobots actuated by HDM.

2 Design and fabrication

2.1 Design principle

This section introduces the conceptual and mechanical design of the underwater minirobots actuated by HDM. Fig. 1a illustrates the detailed structure and corresponding dimensions of the minirobots, including the combustion actuator, propeller thrusters, and shell. The combustion actuator is designed with a pipe to input premixed gas (oxygen and propane) in certain ratios, a chamber to provide the space for premixed gas storage and reaction, a spark ignitor for combustion inspiration, and a soft membrane (i.e., a hyperelastic membrane) to generate rapid, strong, and recoverable deformations (Fig. 1b). Note that all the required electronic components (e.g., the single-chip microcomputer (SCM), battery, and wires) are organized and stored in the shell. The working principle of the combustion actuator can be summarized as follows: propane and oxygen gas is released from the gas cylinders and then accurately premixed by the electronic flow meter. After feeding the premixed gas into the chamber, combustion ignition can be triggered by the high voltage release phenomenon at the generator tip. The dramatic pressure changes in the chamber transiently expand the soft membrane into volcano-like shapes within ~9 ms (Yang et al., 2020), which powerfully push against the ground for rapid underwater jumps. The process from initiation to expansion of the soft membrane is the response process driven by combustion, and the response time is the indicator of reaction ability (Wang et al., 2021). Fig. 1c shows the rigid actuation principle of the minirobots driven by the propeller thrusters. Namely, clockwise counter-acting torques are produced by $\boldsymbol{M}_2$ and $\boldsymbol{M}_4$, and anticlockwise counter-acting torques are produced by $\boldsymbol{M}_1$ and $\boldsymbol{M}_3$. The minirobots are powered by 9-V direct-current (DC) voltage. The rotational direction and speed of the propellers are controlled by the electrical speed controllers (ESCs). To realize the rising, hovering, and drifting motion modes, the propulsion strategies of the propellers are designed as follows: In the rising mode, the increase in the rotational speed of the propellers overcomes the robot's weight to perform lifting. In the hovering mode, the lifting reaches the force's equilibrium for the minirobots. In the drifting mode, horizontal thrusts are produced by setting different rotational speeds for the offside propellers. Fig. 1d presents a flowchart of the HDM. The SCM timing program, gas amount, and ESC parameters are preset, and correspond to T_1, T_2, V_{gas}, and $\boldsymbol{F}_{1\text{–}4}$ in the initial parameter, where T_1 is the actuation time of combustion, T_2 is the actuation time of propulsion, V_{gas} is the gas amount, and $\boldsymbol{F}_{1\text{–}4}$ is the propulsion force. The timing program in the SCM is written so as to control the channel switch of the connected relay, and the relay controls the start and stop of the actuation. The initial conditions, consisting of T_1, T_2, V_{gas}, and $\boldsymbol{F}_{1\text{–}4}$, are experimentally pre-determined to accurately control different motion modes. Jumping is generated by the deformation of the soft membrane due to combustion at T_1 and propulsion is generated by the propellers starting at T_2. The SCM functions as the control center to accurately separate these initial conditions.

2.2 Motion modes of the minirobots

Analyses of the motion strategies of the minirobots are shown in Fig. 2a. The rising, drifting, and hovering modes are defined as $\theta \leqslant 10°$, $45° \leqslant \theta \leqslant 55°$, and $\theta \leqslant 10°$, respectively, to quantitatively specify these three modes (Figs. 2a, 2b, and 2c). In addition, $\frac{\Delta x}{\Delta y} \leqslant$

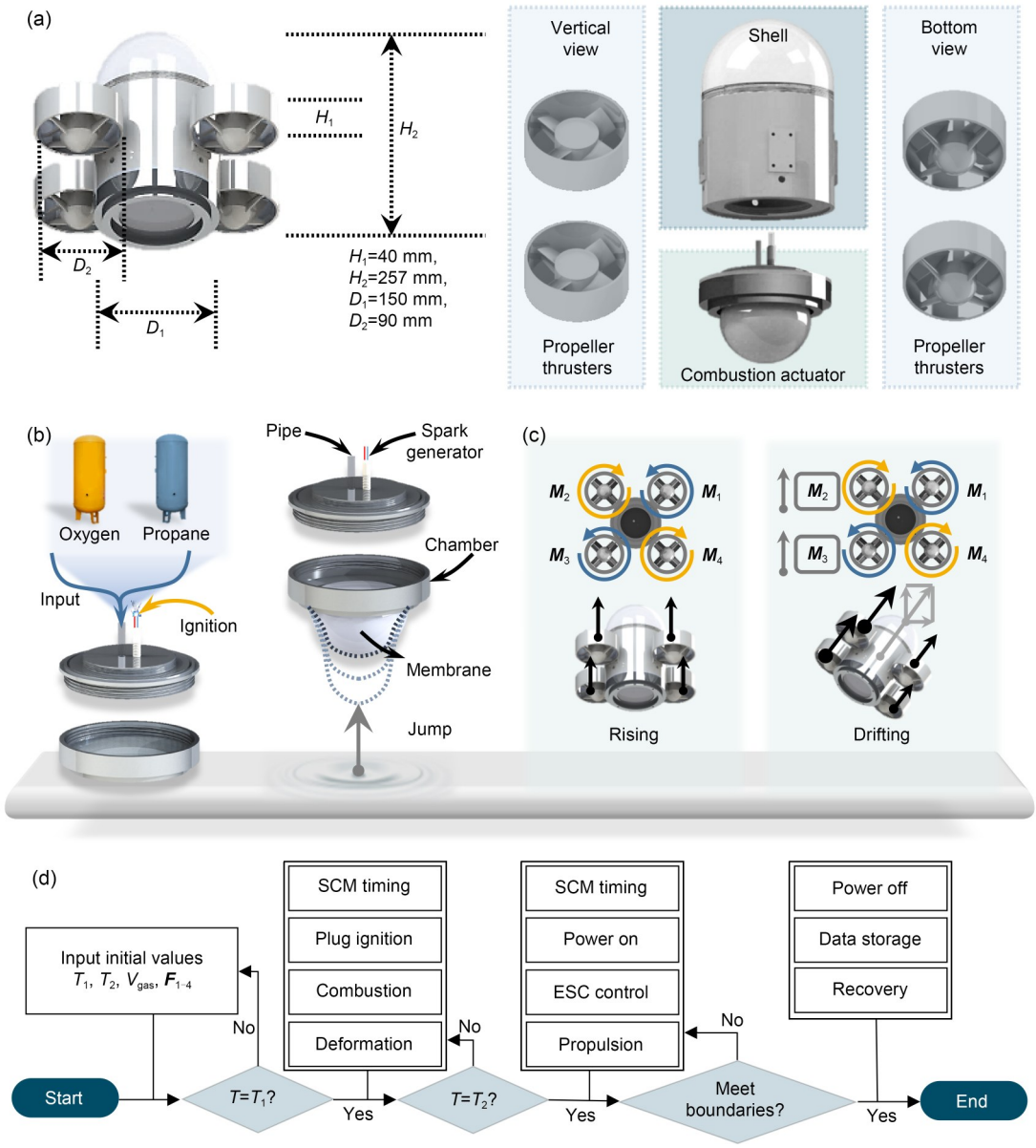

Fig. 1 Design principle and dimensions of the underwater minirobots actuated by HDM: (a) overall design and dimensions of the minirobots; (b) structures and the actuation principle of the combustion actuator; (c) propulsion principle of the propeller thrusters; (d) flowchart illustrating the control principle of the robot actuated by HDM. *T* is the time of the motion process

0.1, $\frac{\Delta x}{\Delta y}\geqslant 0.5$, and $\Delta y \leqslant H_{\text{Robot}}$ are defined for the three modes, respectively. θ, Δx, Δy, and H_{Robot} are the deflection angle, the horizontal displacement, the vertical displacement, and the height of the robot, respectively.

2.3 Fabrication

Table 2 presents the geometric parameters and material properties of the HDM minirobots. The fabrication process (Fig. 3) is divided into three steps: molding fabrication of membranes, 3D printing of the main body, and assembly of the fabricated components and electronic devices. The molding fabrication process contains five steps (Fig. 3a): (1) equal amounts (70 mL) of Dragon Skin 30 silicon rubber gels A and B are poured into a beaker (Yang et al., 2020). (2) An agitator is applied to stir and fully mix the gels. (3) The mixture is perfused into a 3D-printed mold. (4) A vacuum generator is applied to deform and eliminate any bubbles in the soft membranes. (5) The mixture is

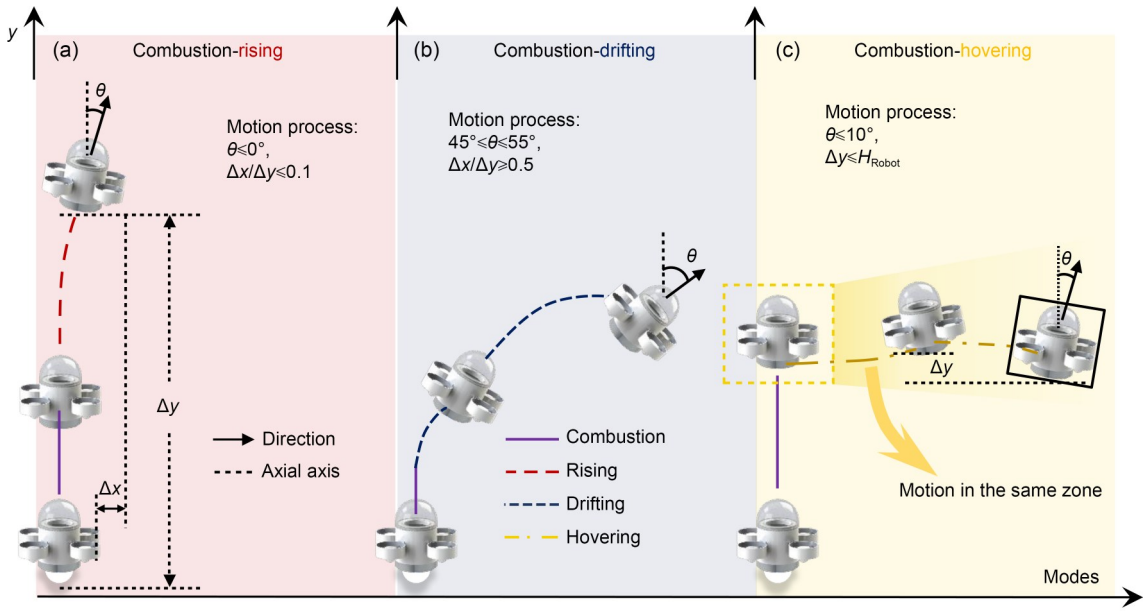

Fig. 2 Motion strategies and quantitative definitions of the three planned motional modes: (a) rising mode; (b) drifting mode; (c) hovering mode. References to color refer to the online version of this figure

Table 2 Detailed dimensions of components

Component	Parameter	Value
Membrane	Diameter (mm)	140
	Thickness (mm)	8
	Effective diameter (mm)	120
	Young's modulus (MPa)	0.3
	Poisson's ratio	0.48
	Cure time (h)	8
Robot body	Diameter (mm)	150
	Height (mm)	257
	Young's modulus (MPa)	3000
	Poisson's ratio	0.4
Propeller thrusters	Rated voltage (V)	12
	Maximum speed (r/min)	5500

cured at normal room temperature (25 °C) for more than 8 h.

The HDM minirobots comprise a head, shell, propellers, motors, SCM, ESCs, chamber cover, and chamber base (Fig. 3b). The head and shell, fabricated with the polylactic acid (PLA) material, contain hollows to provide spaces for the power supply and other electronic components. The material properties of the PLA material can be found in Table 2. PLA material used for 3D printing has high biocompatibility and degradability, is non-toxic to humans, and can directly enter soil organic matter or be absorbed by plants. According to the material properties and the structural parameters of the robot, we estimated the bearable pressure of the robot to be ~1.08 MPa and the maximum working depth to be ~108 m. The propeller thrusters are evenly installed on the shell in the circumferential direction. Two mounting holes are designed on the top surface of the chamber cover to assemble the gas tube and spark generator.

3 Experimental study

In this section, we describe experimental studies conducted following the three motion modes set above, aiming to verify: (1) rapidity in underwater motion, i.e., a superior actuation acceleration and response time by combustion actuators, (2) continuity in underwater motion, i.e., a continuous and stable driving force provided by continuous propeller thrusters, and (3) controllability in underwater motion, i.e., the trajectory of the robot within the preset parameter range.

3.1 Experimental setup

In this section we introduce the experimental setup of the underwater testing for the HDM minirobots. The equipment comprised a recording system, testing environment, and gas system. Fig. 4a shows the setup of the recording system that consisted of a high-speed camera with a speed of up to 12000 frame/s, a corresponding personal computer (PC) to store the large

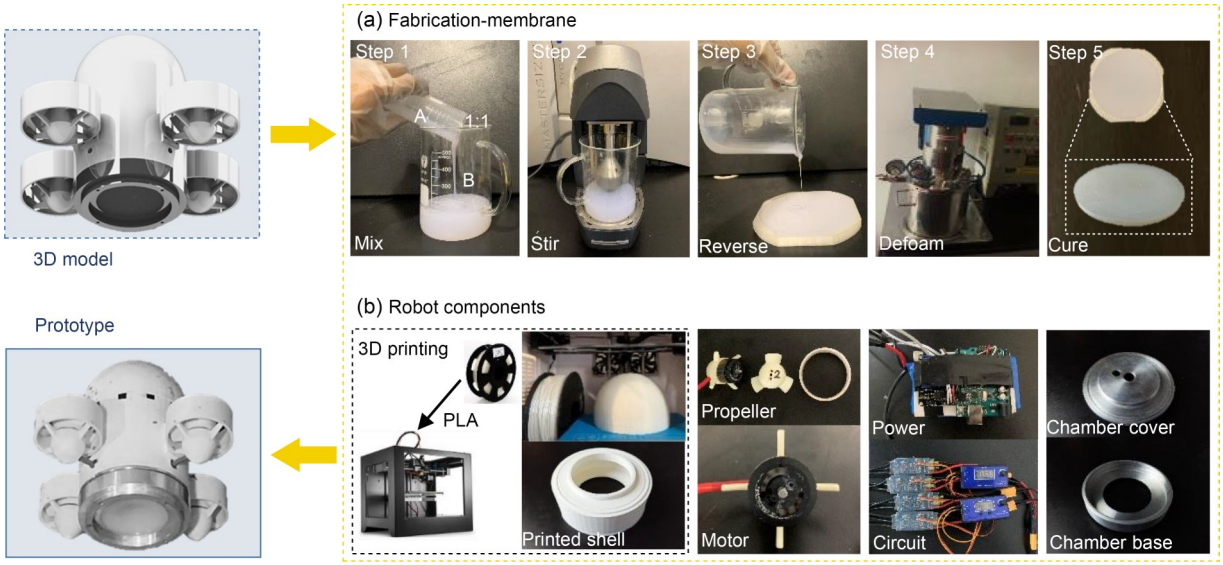

Fig. 3 Fabrication processes of the underwater minirobots: (a) five fabrication processes of the soft membrane; (b) 3D-printed head and shell, electronics (i.e., propeller, motor, SCM, and ESC), and chamber cover and base in the HDM minirobots. PLA represents the polylactic acid

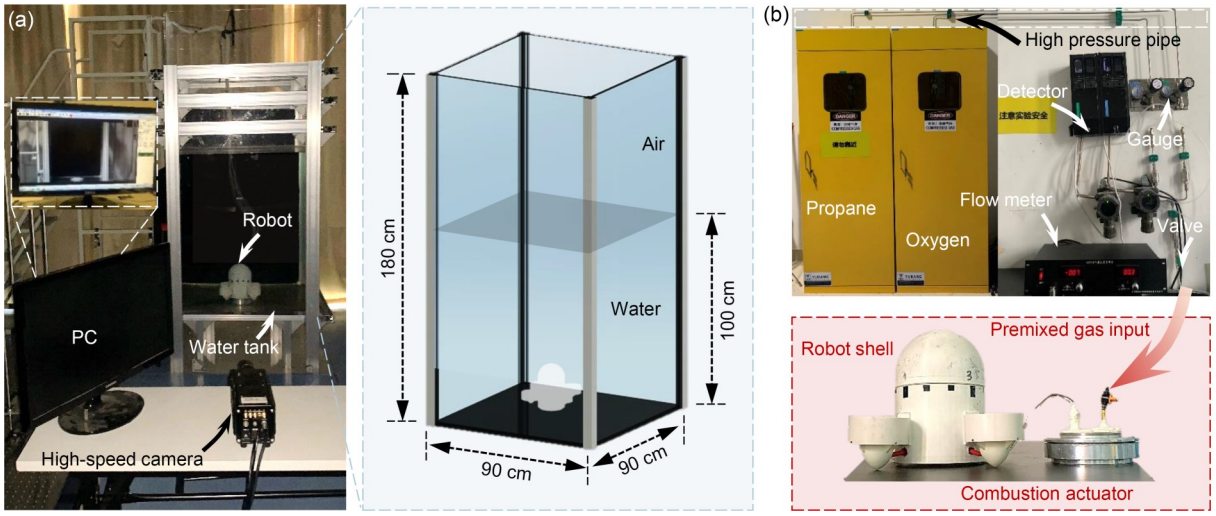

Fig. 4 Experimental setup of the underwater soft robots: (a) setup for the underwater testing platform; (b) setup for gas input system

amount of image data and for switching the camera, a water tank placed in front of the camera, and the HDM minirobots set at the bottom of the water tank. Fig. 4a also shows the testing environment setup. The water tank was 0.9 m long, 0.9 m wide, and 1.8 m high, and held water up to 1 m deep. Given the body height of 257 mm for the minirobots (Fig. 1a), the water tank provided a motion range of 4 times the robot height. The gas system setup (Fig. 4b) contained an explosion-proof cabinet for storing the oxygen and propane cylinders, two high-pressure pipelines used to transmit these two gases, pressure gauges, check valves, flame arresters, and an electronic flow meter that accurately controlled input gas amounts. The oxygen and propane were mixed by the gas system and air, and fed into the chamber through the input tube of the combustion actuator.

3.2 Experiment results

To investigate the kinematic performance of the HDM minirobots, motions generated by different gas amounts and durations were captured by the high-speed

camera (Table 3). The captured images were automatically processed in MATLAB by the binarization method to obtain outlines of the minirobots. By recognizing the changes in position of the minirobots between the captured images, motion trajectories were accurately obtained (Figs. 5–7). Performance records for the three motion modes are provided in Videos S1–S3 of the ESM.

Table 3 Experimental case table

Case No.	Motional mode	Gas volume, V_{gas} (mL)	Time duration, ΔT (ms)
1	Rising	20	200
2	Rising	25	500
3	Rising	30	800
4	Drifting	20	200
5	Drifting	25	500
6	Drifting	30	800
7	Hovering	20	800

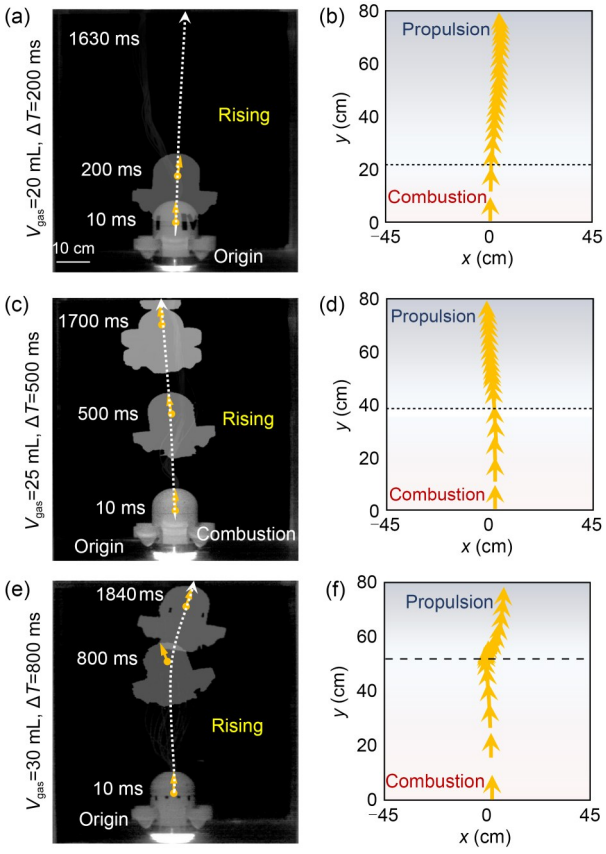

Fig. 5 Experimental results of the HDM minirobots in the rising mode. Captured images (a, c, and e) and processed trace vectors (b, d, and f) showing the kinematic performance under the cases of V_{gas}=20 mL, ΔT=200 ms (a and b), V_{gas}=25 mL, ΔT=500 ms (c and d), and V_{gas}=30 mL, ΔT=800 ms (e and f)

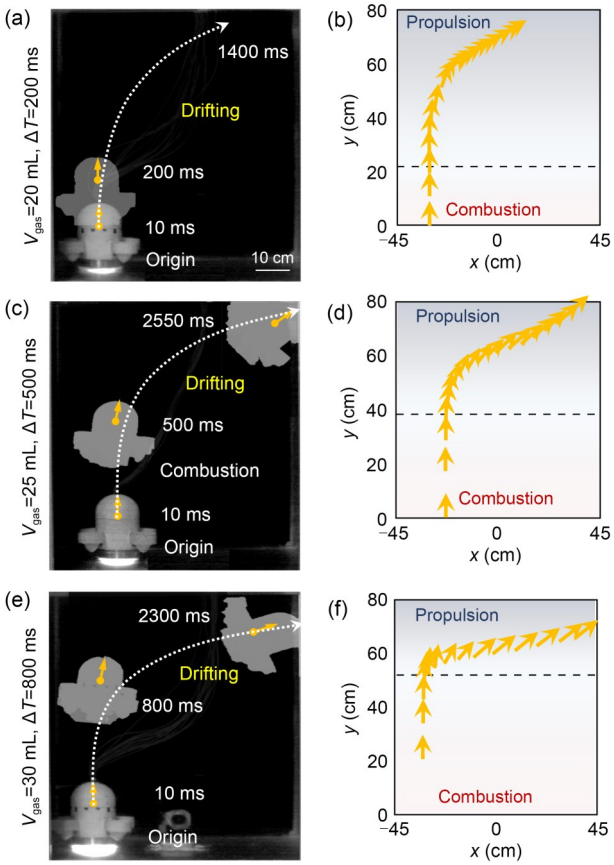

Fig. 6 Experimental results of the HDM minirobots in the drifting mode. Captured images (a, c, and e) and processed trace vectors (b, d, and f) showing the kinematic performance under the cases of V_{gas}=20 mL, ΔT=200 ms (a and b), V_{gas}=25 mL, ΔT=500 ms (c and d), and V_{gas}=30 mL, ΔT=800 ms (e and f)

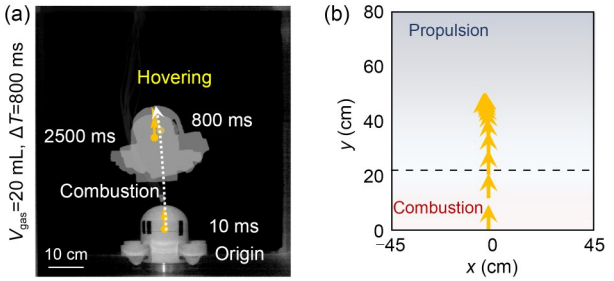

Fig. 7 Experimental results of the HDM minirobots in the hovering mode. Captured images (a) and processed trace vectors (b) showing the kinematic performance under the case of V_{gas}=20 mL, ΔT=800 ms

Fig. 5 presents the results of the rising mode with respect to the premixed gas amounts V_{gas} and time durations ΔT. When $V_{gas}=20$ mL and $\Delta T=200$ ms (Figs. 5a and 5b), the minirobots transiently jump upward (within 10 ms) by combustion. Propeller thrusters are automatically switched on at 200 ms, leading

to a smooth rising motion. Afterward, the minirobots continue rising until they reach the water surface at 1630 ms. When $V_{gas}=25$ mL and $\Delta T=500$ ms (Figs. 5c and 5d), the minirobots jump up with higher speed due to the increased premixed gas amount. The propellers are activated at 500 ms, and inconspicuous pauses are observed during the switching process. The minirobots finally reach the water surface at 1700 ms, showing a reduced actuation efficiency. When $V_{gas}=30$ mL and $\Delta T=800$ ms (Figs. 5e and 5f), the minirobots jump up dramatically in 10 ms, and the propeller thrusters are switched on at 800 ms. Unlike in the former cases, the motions under this condition present obvious pauses during the switching process. Instead of improving the kinematic performance, combustion has brought unsteadiness to the overall motions due to the excessive time duration (i.e., $\Delta T=800$ ms).

Fig. 6 presents the results of the drifting mode with respect to the premixed gas amounts V_{gas} and time durations ΔT. When $V_{gas}=20$ mL and $\Delta T=200$ ms (Figs. 6a and 6b), the propeller thrusters start working at 200 ms with differential speeds after jumping. The minirobots perform the rotation phenomenon to adjust their motional direction to horizontal.

Due to the early activation of the propeller actuation, the minirobots reach the water surface before the completion of the rotation process. When $V_{gas}=25$ mL and $\Delta T=500$ ms (Figs. 6c and 6d), the propellers start working at 500 ms, adjusting the orientation of the minirobots until they reach the boundary at 2550 ms. When $V_{gas}=30$ mL and $\Delta T=800$ ms (Figs. 6e and 6f), the minirobots jump up dramatically. The propeller thrusters are switched on to let them move horizontally. The trajectory of the minirobots can be adjusted by changing the premixed gas amount and time duration.

Fig. 7 presents the results of the hovering mode. After the same combustion actuation process as the rising and drifting modes when $V_{gas}=20$ mL, the propulsion process is started at 800 ms to provide a lower thrust force, leading to a force equilibrium to maintain hovering. The experimental results showed that the HDM minirobots can achieve fast and flexible underwater motion performance.

In addition, we conducted experiments in a dynamic fluid environment to further verify the motion performance of the underwater minirobots. Fig. 8a shows the flume setup. The flow velocity v_w and input gas amount were set to v_w=0.4 m/s, V_{gas}=20 mL, respectively.

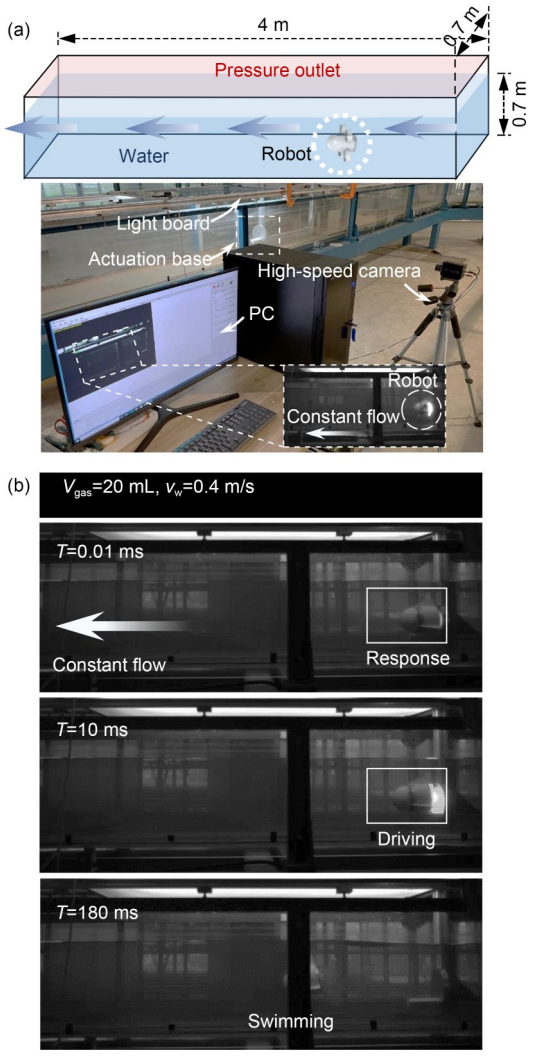

Fig. 8 Experimental results of the minirobots in the dynamic fluid environment: (a) construction of the test platform setup; (b) captured images showing the kinematic performance under the case of V_{gas}=20 mL, v_w=0.4 m/s

Fig. 8b shows the testing process. The experimental results showed that the response time (~9 ms) and the actuation acceleration (~10 m/s^2) of the robot in the dynamic fluid environment were consistent with those in a stationary pool (Wang et al., 2023).

4 Model validation

4.1 Numerical modeling and results

The kinematic performance of the HDM minirobots was numerically simulated in ANSYS Fluent (Adam et al., 2017), as shown in Fig. 9a. The simulation method is based on a fluid–solid coupling strategy

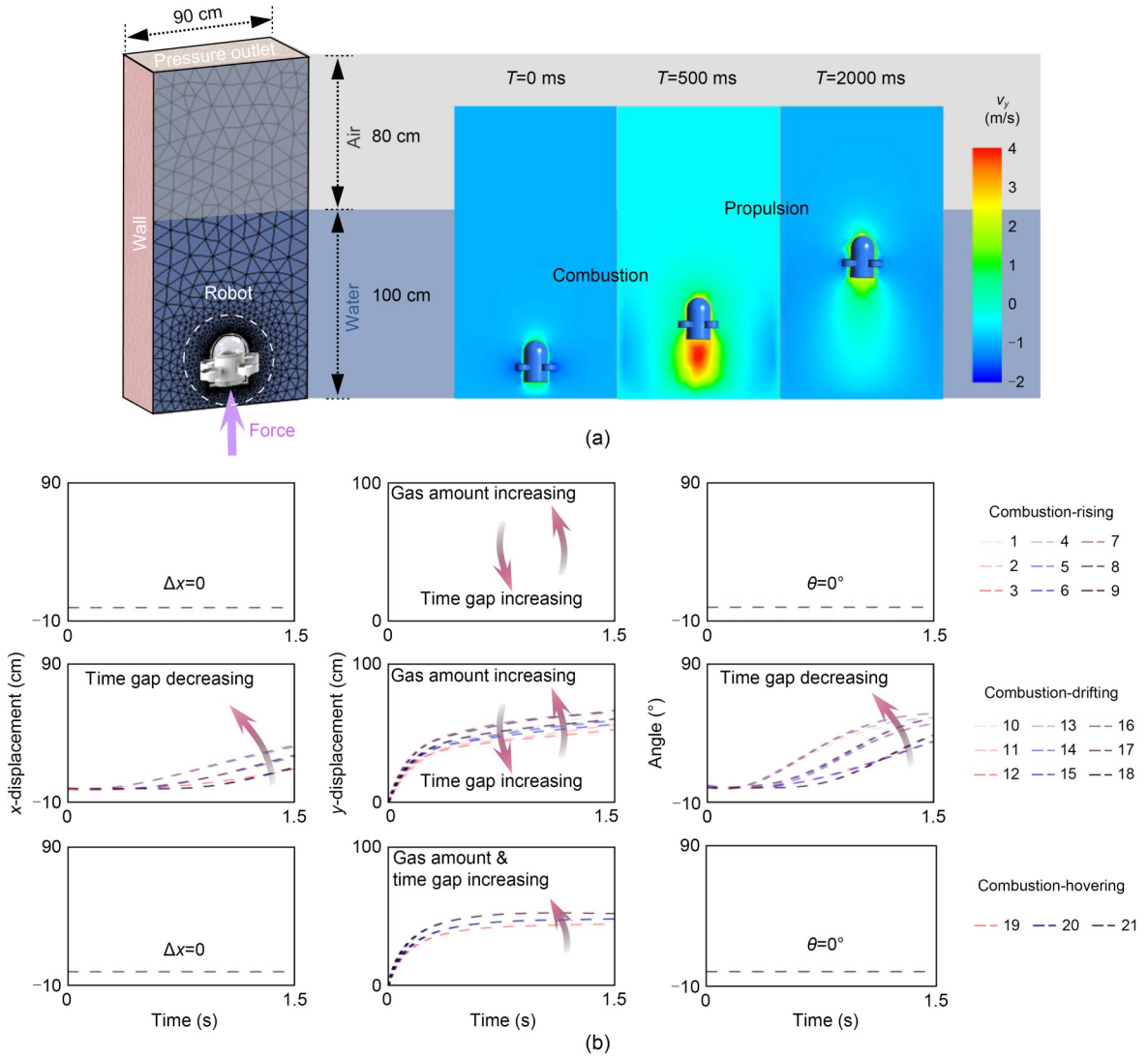

Fig. 9 Numerical modeling of the underwater minirobots actuated by HDM: (a) setup of the numerical models and the simulated motions of the minirobots in the rising mode; (b) numerical results of the minirobots in the rising, drifting, and hovering modes. v_y is the velocity of the robot in the vertical direction. References to color refer to the online version of this figure

that combines the mechanical analysis of a solid object (i.e., minirobots) with the fluid dynamic analysis of a disturbed flow field. Since the minirobots are undeformable, they can be simplified as a rigid object propelled by the combustion thrust force against the wall of the tank, which transiently disturbs the environmental field. The spring and remeshing methods were selected to ensure calculation accuracy, i.e., the mesh was given deformation tolerances and the global mesh was remeshed when the deformation exceeded the tolerances, respectively. Table 4 presents the detailed parameters of the numerical model and Table 5 the case table of the numerical simulation. The kinematic performance calculated by the developed numerical models is shown in Fig. 9b. Further results are given in Videos S4–S6 of the ESM.

In the rising mode, the minirobots jump upward rapidly during T=0–200 ms, actuated by explosive thrust forces generated by combustion. During T=200–1500 ms, the velocity of the minirobots is significantly reduced due to drag. The displacements in the y-direction are increased with the increment of V_{gas} and decreased with the increment of ΔT. However, the displacements in the x-direction and deflection angles are ideally calculated as constants (i.e., 0 mm and 0°). In the drifting mode, the x-direction displacements

Table 4 Parameters used in the numerical simulations

Item	Parameter	Description
Mesh	Number of nodes	8368
	Number of elements	44854
	Element size (mm)	114.46
	Maximum size (mm)	228.91
Dynamic mesh	Spring constant factor	0.7
	Number of iterations	100
	Max cell skewness	0.91
	Remeshing interval	1
Viscous model	Model	Standard k-ε
	C_μ	0.090
	$C_{1\varepsilon}$	1.440
	$C_{2\varepsilon}$	1.920
	σ_k	1
	σ_ε	1.300
Solution method	Scheme	PISO
	Neighbor correction	1
	Skewness correction	1

C_μ, $C_{1\varepsilon}$, and $C_{2\varepsilon}$ are constant terms. σ_k and σ_ε are the turbulence Prandtl numbers of the k and ε equations, respectively. PISO is an algorithm called pressure-implicit with splitting of operators

Table 5 Numerical case table

Case No.	φ (N)	F_T	V_{gas} (mL)	ΔT (ms)
1/2/3	4000	3 N×4	20	200/500/800
4/5/6	4400	3 N×4	25	200/500/800
7/8/9	5200	3 N×4	30	200/500/800
10/11/12	4000	3 N×2+0.75 N×2	20	200/500/800
13/14/15	4400	3 N×2+0.75 N×2	25	200/500/800
16/17/18	5200	3 N×2+0.75 N×2	30	200/500/800
19/20/21	4000	0.25 N×4	20	800/1100/1400

φ is the peak value of the combustion thrust; F_T is the thrust force

and deflection angles are independent of V_{gas}, and are increased and decreased, respectively, with the increment of ΔT. In the hovering mode, the hovering state is directly determined by V_{gas}. To reach the hover state, once V_{gas} is selected, ΔT is correspondingly determined.

4.2 Theoretical modelling and results

A theoretical analysis model of motion process of the HDM minirobots was developed. The driving process can be divided into three stages, i.e., the combustion process, deceleration process, and propulsion process. In the combustion process, the force equilibrium can be shown as

$$\boldsymbol{F}_C=\boldsymbol{G}-\boldsymbol{F}_B+\boldsymbol{F}_D+\boldsymbol{F}_R+\boldsymbol{F}_A,\quad T\in[0,\lambda_1], \tag{1}$$

where $\boldsymbol{F}_C$, $\boldsymbol{G}$, $\boldsymbol{F}_B$, $\boldsymbol{F}_D$, $\boldsymbol{F}_R$, and $\boldsymbol{F}_A$ are the thrust force generated by combustion, gravity of the minirobot, buoyancy of the robot, drag force, resultant force, and added mass, respectively. λ_1 is the end time of the combustion process. F_C can be calculated as (Yang et al., 2020; Wang et al., 2021)

$$F_C=\varphi\cdot\cos(180T). \tag{2}$$

φ is presented in Table 5. $\boldsymbol{F}_D$ can be calculated as

$$\boldsymbol{F}_D=\frac{1}{2}C_d\rho_{water}S\boldsymbol{v}^2, \tag{3}$$

where C_d, ρ_{water}, S, and $\boldsymbol{v}$ are the drag coefficient, water density, upstreaming area, and velocity of robot, respectively. $\boldsymbol{F}_A$ can be calculated as

$$\boldsymbol{F}_A=\alpha\rho V\frac{\mathrm{d}\boldsymbol{v}}{\mathrm{d}T}, \tag{4}$$

where α is the added mass coefficient and V is the volume of the robot. The duration time of the combustion process was 8.9 ms (Yang et al., 2020). The deceleration process can be described as

$$\boldsymbol{0}=\boldsymbol{G}-\boldsymbol{F}_B+\boldsymbol{F}_D+\boldsymbol{F}_R+\boldsymbol{F}_A,\quad T\in[\lambda_1,\lambda_2]. \tag{5}$$

The end time of the deceleration process λ_2 can be calculated as

$$\lambda_2=T_2-T_1-\lambda_1. \tag{6}$$

All the motion modes were distinguished by the propulsion process. In the rising and hovering modes, the propulsion process can be described as

$$\boldsymbol{F}_T=\boldsymbol{G}-\boldsymbol{F}_B+\boldsymbol{F}_D+\boldsymbol{F}_R+\boldsymbol{F}_A. \tag{7}$$

Note that the difference between the rising and hovering modes is the value of $\boldsymbol{F}_T$ (Table 5). In the drifting mode, the motion in a 2D plane can be described as

$$\begin{cases} \boldsymbol{F}_{Tx} = \boldsymbol{F}_{Dx} + \boldsymbol{F}_{Rx} + \boldsymbol{F}_{Ax}, \\ \boldsymbol{F}_{Ty} = \boldsymbol{G} - \boldsymbol{F}_{B} + \boldsymbol{F}_{Dy} + \boldsymbol{F}_{Ry} + \boldsymbol{F}_{Ay}, \end{cases} \tag{8}$$

where the subscripts x and y indicate the horizontal and vertical directions, respectively.

The kinematic performance of the HDM minirobots can be theoretically obtained by solving Eqs. (1)–(8). Figs. 10a and 10b illustrate the relationships between the premixed gas amount, time, activation time of the thrusters, and the x-displacement. During 0–1.5 s, the deflection angles, premixed gas amount, and actuation time gap are compared between the two driving methods, which are ranged as $x\in[0, 35]$ cm, $y\in[0, 80]$ cm, $\theta\in[0°, 60°]$, $V_{gas}\in[20, 30]$ mL, $\Delta T\in[0.2, 0.8]$ s, respectively. Depending on the propulsion duration, the x-displacement and deflection angle are significantly decreased when ΔT is increased from 0.2 s to 0.8 s (V_{gas} is 25 mL). The x-displacement and deflection angle are sustained as V_{gas} is changed at ΔT=0.5 s, mainly due to the relationship between the rotation phenomenon and the propellers' thrust. The y-displacement is increased as V_{gas} is changed from 20 mL to 30 mL at ΔT=0.5 s, due to the dominant effect of V_{gas} on y-displacement.

The HDM-driven minirobots reported in this study are characterized mainly by their underwater actuation performance, so this study focused mainly on the results from the test experiments. Since the numerical simulations and theoretical modelling were used only to validate the experimental results, the theoretical model may not be suitable for wider use. In a recent publication, we have developed a comprehensive theoretical model to analyze the actuation performance of HDM-driven minirobots (Yang et al., 2022).

4.3 Comparison and validation

The experimental, numerical, and theoretical results of the minirobots were compared (Fig. 11). In particular, the motion positions at 1.5 s were compared under different premixed gas amounts V_{gas} and time gaps ΔT between combustion and propulsion. In the rising mode, the minirobots could be lifted by combustion by an average of 76.8 cm and a maximum of 92.4 cm. In the drifting mode, they could be lifted by 63.2 cm with a maximum of 71.5 cm and drift laterally for an average of 23.1 cm and a maximum of 36.4 cm. In the hovering mode, they could be lifted and hover at a certain height for 44.8 cm with a maximum

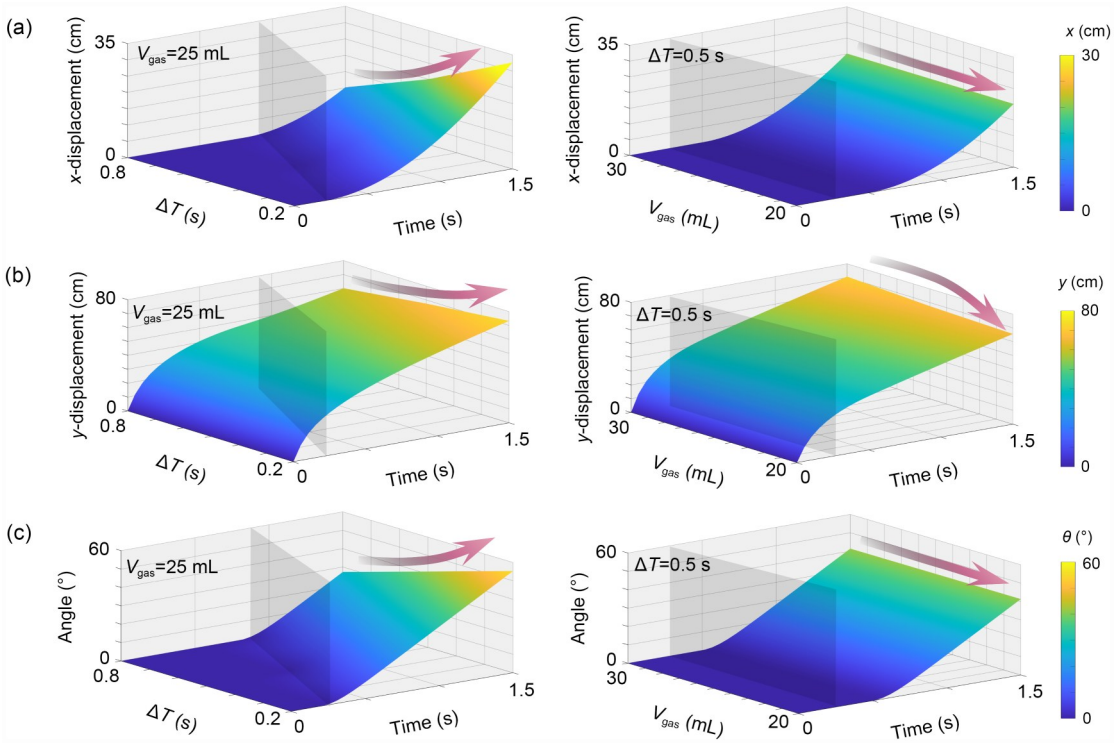

Fig. 10 Theoretical results in the condition of drifting mode (V_{gas}=25 mL, ΔT=0.5 s): (a) horizontal displacements; (b) vertical displacements; (c) deflection angles. References to color refer to the online version of this figure

of 49.2 cm. Although the factors such as unstable combustion and the center-of-gravity shift may slightly affect the accuracy of the experimental results, the overall differences among the comparisons in this study were only about 10%, which is acceptable.

5 Locomotion performance

Fig. 12 summarizes and compares our proposed method with existing hybrid driving technologies enabled by combustion (Tolley et al., 2014a; Zi et al., 2016), SMP (Schmidt, 2006; McCoul et al., 2017), magnets (Sadeghzadeh et al., 2012; Li et al., 2016; Chen et al., 2018), EM (Mohd Said et al., 2017; Tone and Suzuki, 2018), gels (Shin et al., 2008; Yue et al., 2013; Zhang et al., 2013; Kadiyam and Mohan, 2019; Gu et al., 2020), and thrusters (Stokes et al., 2014; Kim et al., 2017; Zhang et al., 2021). The HDM minirobots reported in this study performed with satisfactory operational reliability and transient actuation ability. Combustion-based actuation is able to address the challenges of instantaneous rapid starting, and the propeller-based actuation is able to address the challenges of motion performance. The drawbacks of previous propeller-based technologies are their longer actuation time and lower driving speed (Stokes et al., 2014; Kim et al., 2017; Zhang et al., 2021). The disadvantages of the published combustion driving methods are their relatively low control accuracy due to the over-transient driving time and the discontinuous driving force (Tolley et al., 2014a; Zi et al., 2016). The HDM could be a potential solution to address the issues of both actuation methods by offering transient actuation and a sustained driving force. Fig. 12 also compares the dimensions of the devices in those studies, which ranged from the millimeter to centimeter scales. In particular, the HDM minirobot bodies are about 30 mm high (Table 1). Increasing the overall size of HDM to the meter scale, the estimated combustion-based driving

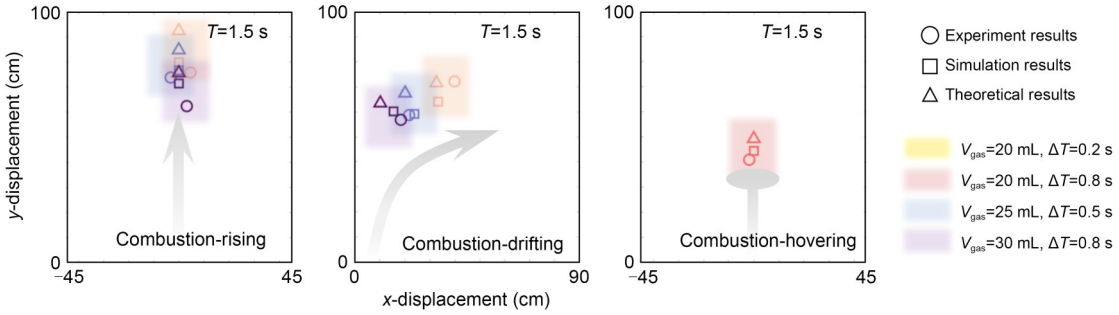

Fig. 11 Comparison of the motion performance between the experimental, numerical, and theoretical results. The motion performance was investigated with respect to the gas amount and time gap between the rising, drifting, and hovering modes. References to color refer to the online version of this figure

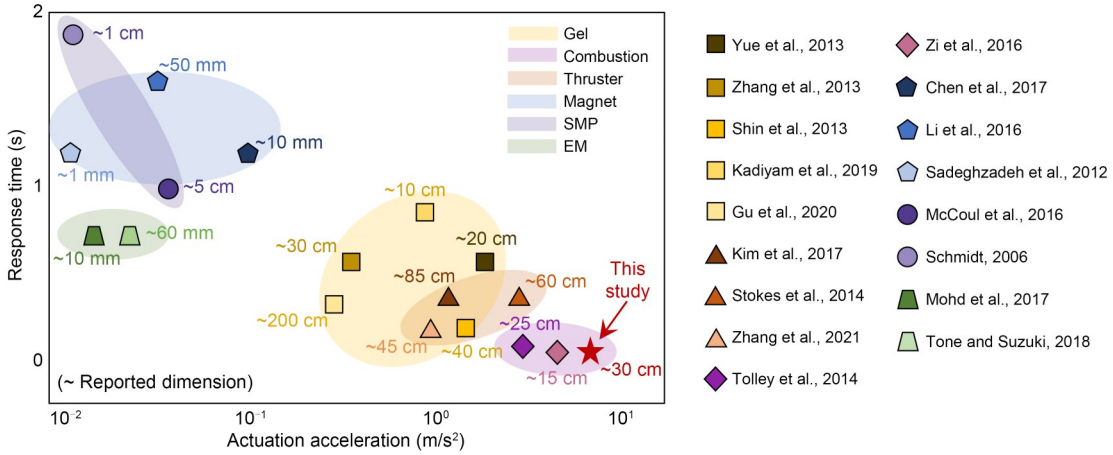

Fig. 12 Comparison between the reported HDM and the selected driving technologies in previous studies, including gel, combustion, thruster, magnet, SMP, and EM. References to color refer to the online version of this figure

force would be 100 kN with an actuation velocity of 10 m/s, while the propeller-based driving force would be about 20 kN in total with a velocity of 3 m/s. As a consequence, the main contribution of our HDM method is the combination of combustion with propellers to achieve superior motion performance.

1. Rapidity in underwater motion. Traditional driving methods (e.g., multi-propeller cooperative propulsion, hydraulic propulsion, vector propulsion, and waterjet propulsion) typically achieve ~3 m/s^2 in actuation acceleration and ~0.2 s in response time. However, many applications require transient reactions (e.g., underwater transient starting and braking, escaping from being stuck, instantaneous obstacle avoidance, and instantaneous steering). In our previous study, we reported the TDM actuated by combustion, which could achieve an actuation acceleration of ~10 m/s^2 and a response time of ~0.01 s (Jiao et al., 2023).

2. Continuity in underwater motion. The TDM has severe limitations with continuous driving. However, many applications require continuous motion. Propeller thrusters make up for the deficiency of continuity in the TDM, providing a continuous and stable driving force.

3. Controllability in underwater motion. The HDM developed in this study combines conventional driving methods with TDM, i.e., it combines combustion-based actuators with propeller thrusters to provide a promising powering technique for application to underwater robots in ocean engineering. The HDM-enabled underwater minirobots can achieve accurate, fast, and flexible underwater locomotion performance. In the experimental tests, the trajectory of the robot was within the preset parameter range. This class of HDM, comprising hard and soft actuation functioning synergistically, is capable of performing tasks that neither can do alone.

6 Limitations and future work

Although the minirobots perform promisingly with HDMs in a hydrostatic environment, testing in real complex fluid environments has not been conducted, and there has been limited development of functional applications. As a follow-up study, the design and algorithm of the underwater robots are now being optimized and will be tested in a field environment for further industrial applications. The combination of artificial intelligence (AI) with the new robot would allow deep learning to be applied to the design and use of robots. In addition, it is necessary to develop a variety of underwater operation functions for the robot, such as monitoring, human-robot interaction, target recognition, and grasping, to further expand the application prospects of robots in the field of engineering (Qi and Aliverti, 2020; Qi et al., 2021).

7 Conclusions

In this study, we investigated the performance of underwater minirobots actuated by an HDM. The HDM minirobots, which are driven by actuations based on combustion and propellers, were investigated in rising, drifting, and hovering modes. Experiments were conducted to test the kinematic performance of the minirobots in the three modes, and the test results indicated that the minirobots are able to transiently jump by combustion and then keep rising, steering or remaining stable at a certain location in the three modes. Numerical models were developed to investigate the hydrodynamic-coupled mechanical process, and theoretical models were established to quantitatively study the mechanics of the driving process. Experimental, numerical, and theoretical results were compared, and showed satisfactory agreement. The motion performance of the HDM minirobots (i.e., acceleration and response time) was compared with that of existing hybrid actuation technologies. The results showed that the HDM minirobots have good operation reliability and transient actuation ability. Considering the characteristics of transient velocity movement actuated by combustion, many application prospects (e.g., underwater transient starting and braking, escaping from being stuck, instantaneous obstacle avoidance, and instantaneous steering) in underwater scenarios could involve the use of these minirobots. Propeller thrusters make up for the deficiencies of accuracy and maneuverability in combustion, provide a continuous and stable driving force, and have potential applications, such as underwater monitoring in the potential application scenario (Fig. 13). The reported HDM combines the advantages of a transient response and underwater propellers to achieve more flexible and controllable motion performance, and represents a promising powering technique for application to underwater robots in ocean engineering.

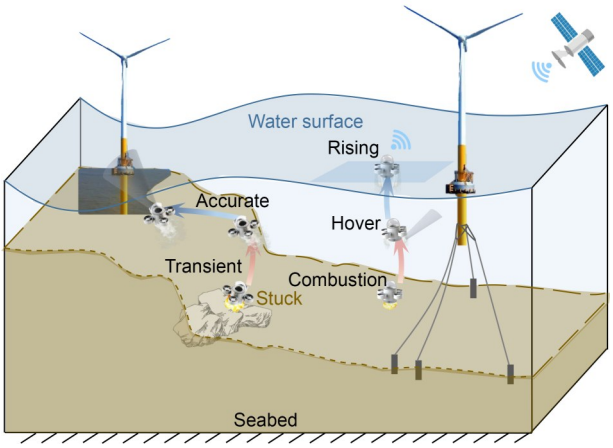

Fig. 13 Potential applications of underwater minirobots actuated by HDMs

Acknowledgments

This study is supported by the Key Research and Development Plan of Zhejiang Province, China (No. 2021C03181), the Startup Fund of the Hundred Talents Program at the Zhejiang University, China, and the China Scholarship Council (No. 202006320349).

Author contributions

Xinghong YE and Pengcheng JIAO designed the research. Lingwei LI and Xinghong YE conducted the experiments. Yang YANG proposed the theoretical model. Xinghong YE, Lingwei LI, and Yang YANG processed the numerical data. Xinghong YE and Yang YANG wrote the first draft of the manuscript. Zhiguo HE revised and edited the final version.

Conflict of interest

Xinghong YE, Yang YANG, Pengcheng JIAO, Zhiguo HE, and Lingwei LI declare that they have no conflict of interest.

References

Adam SAA, Zhou JP, Zhang YH, 2017. Modeling and simulation of 5DOF robot manipulator and trajectory using MATLAB and CATIA. Proceedings of the 3rd International Conference on Control, Automation and Robotics, p.36-40. https://doi.org/10.1109/ICCAR.2017.7942657

Albiez J, Joyeux S, Gaudig C, et al., 2015. FlatFish–a compact subsea-resident inspection AUV. OCEANS-MTS/IEEE Washington, p.1-8. https://doi.org/10.23919/OCEANS.2015.7404442

An RC, Guo SX, Gu SX, et al., 2019. Improvement and evaluation for the stability of mobile spherical underwater robots (SUR III). IEEE International Conference on Mechatronics and Automation, p.2512-2517. https://doi.org/10.1109/ICMA.2019.8816247

Antonelli G, Caccavale F, Chiaverini S, 2004. Adaptive tracking control of underwater vehicle-manipulator systems based on the virtual decomposition approach. *IEEE Transactions on Robotics and Automation*, 20(3):594-602. https://doi.org/10.1109/TRA.2004.825521

Banerjee H, Suhail M, Ren HL, 2018. Hydrogel actuators and sensors for biomedical soft robots: brief overview with impending challenges. *Biomimetics*, 3(3):15. https://doi.org/10.3390/biomimetics3030015

Chen GM, Liu A, Hu JH, et al., 2020. Attitude and altitude control of unmanned aerial-underwater vehicle based on incremental nonlinear dynamic inversion. *IEEE Access*, 8:156129-156138. https://doi.org/10.1109/ACCESS.2020.3015857

Chen YH, Wan F, Wu T, et al., 2018. Soft-rigid interaction mechanism towards a lobster-inspired hybrid actuator. *Journal of Micromechanics and Microengineering*, 28(1):014007. https://doi.org/10.1088/1361-6439/aa9e25

Cheng Y, Huang C, Yang D, et al., 2018. Bilayer hydrogel mixed composites that respond to multiple stimuli for environmental sensing and underwater actuation. *Journal of Materials Chemistry B*, 6(48):8170-8179. https://doi.org/10.1039/c8tb02242a

da Cunha MP, Debije MG, Schenning APHJ, 2020. Bioinspired light-driven soft robots based on liquid crystal polymers. *Chemical Society Reviews*, 49(18):6568-6578. https://doi.org/10.1039/D0CS00363H

Das B, Subudhi B, Pati BB, 2016. Co-operative control of a team of autonomous underwater vehicles in an obstacle-rich environment. *Journal of Marine Engineering & Technology*, 15(3):135-151. https://doi.org/10.1080/20464177.2016.1247636

Dinmohammadi F, Flynn D, Bailey C, et al., 2019. Predicting damage and life expectancy of subsea power cables in offshore renewable energy applications. *IEEE Access*, 7:54658-54669. https://doi.org/10.1109/ACCESS.2019.2911260

Gu SX, Guo SX, Zheng L, 2020. A highly stable and efficient spherical underwater robot with hybrid propulsion devices. *Autonomous Robots*, 44(5):759-771. https://doi.org/10.1007/s10514-019-09895-8

He ZG, Yang Y, Jiao PC, et al., 2023. Copebot: underwater soft robot with copepod-like locomotion. *Soft Robotics*, 10(2):314-325. https://doi.org/10.1089/soro.2021.0158

Iscar E, Barbalata C, Goumas N, et al., 2018. Towards low cost, deep water AUV optical mapping. OCEANS MTS/IEEE Charleston, p.1-6. https://doi.org/10.1109/OCEANS.2018.8604772

Jiao PC, Ye XH, Zhang CJ, et al., 2023. Vision-based real-time marine and offshore structural health monitoring system using underwater robots. *Computer-Aided Civil and Infrastructure Engineering*, in press. https://doi.org/10.1111/mice.12993

Kadiyam J, Mohan S, 2019. Conceptual design of a hybrid propulsion underwater robotic vehicle with different propulsion systems for ocean observations. *Ocean Engineering*, 182:112-125. https://doi.org/10.1016/j.oceaneng.2019.04.069

Kim NH, Kim JM, Khatib O, et al., 2017. Design optimization of hybrid actuation combining macro-mini actuators. *International Journal of Precision Engineering and Manufacturing*, 18(4):519-527. https://doi.org/10.1007/s12541-017-0062-z

Laschi C, Mazzolai B, Cianchetti M, 2016. Soft robotics: technologies and systems pushing the boundaries of robot abilities. *Science Robotics*, 1(1):eaah3690. https://doi.org/10.1126/scirobotics.aah3690

Lee C, Kim M, Kim YJ, et al., 2017. Soft robot review. *International Journal of Control, Automation and Systems*, 15(1):3-15. https://doi.org/10.1007/s12555-016-0462-3

Lee H, Xia CG, Fang NX, 2010. First jump of microgel; actuation speed enhancement by elastic instability. *Soft Matter*, 6(18):4342-4345. https://doi.org/10.1039/c0sm00092b

Li GR, Chen XP, Zhou FH, et al., 2021. Self-powered soft robot in the Mariana Trench. *Nature*, 591(7848):66-71. https://doi.org/10.1038/s41586-020-03153-z

Li H, Go G, Ko SY, et al., 2016. Magnetic actuated pH-responsive hydrogel-based soft micro-robot for targeted drug delivery. *Smart Materials and Structures*, 25(2):027001. https://doi.org/10.1088/0964-1726/25/2/027001

Li TF, Li GR, Liang YM, et al., 2017. Fast-moving soft electronic fish. *Science Advances*, 3(4):e1602045. https://doi.org/10.1126/sciadv.1602045

Li WB, Zhang WM, Zou HX, et al., 2018. A fast rolling soft robot driven by dielectric elastomer. *IEEE/ASME Transactions on Mechatronics*, 23(4):1630-1640. https://doi.org/10.1109/TMECH.2018.2840688

Li X, Zhu DQ, Qian YA, 2014. A survey on formation control algorithms for multi-AUV system. *Unmanned Systems*, 2(4):351-359. https://doi.org/10.1142/S2301385014400093

McCoul D, Rosset S, Besse N, et al., 2017. Multifunctional shape memory electrodes for dielectric elastomer actuators enabling high holding force and low-voltage multi-segment addressing. *Smart Materials and Structures*, 26(2):025015. https://doi.org/10.1088/1361-665X/26/2/025015

Mohd Said M, Yunas J, Bais B, et al., 2017. The design, fabrication, and testing of an electromagnetic micropump with a matrix-patterned magnetic polymer composite actuator membrane. *Micromachines*, 9(1):13. https://doi.org/10.3390/mi9010013

Neto EC, Sá RC, Holanda GC, et al., 2014. Autonomous underwater vehicle to inspect hydroelectric dams. *International Journal of Computer Applications*, 101(11):1-11. https://doi.org/10.5120/17728-8801

Qi W, Aliverti A, 2020. A multimodal wearable system for continuous and real-time breathing pattern monitoring during daily activity. *IEEE Journal of Biomedical and Health Informatics*, 24(8):2199-2207. https://doi.org/10.1109/JBHI.2019.2963048

Qi W, Ovur SE, Li ZJ, et al., 2021. Multi-sensor guided hand gesture recognition for a teleoperated robot using a recurrent neural network. *IEEE Robotics and Automation Letters*, 6(3):6039-6045. https://doi.org/10.1109/LRA.2021.3089999

Rus D, Tolley MT, 2015. Design, fabrication and control of soft robots. *Nature*, 521(7553):467-475. https://doi.org/10.1038/nature14543

Sadeghzadeh A, Asua E, Feuchtwanger J, et al., 2012. Ferromagnetic shape memory alloy actuator enabled for nanometric position control using hysteresis compensation. *Sensors and Actuators A: Physical*, 182:122-129. https://doi.org/10.1016/j.sna.2012.05.029

Sahoo A, Dwivedy SK, Robi PS, 2019. Advancements in the field of autonomous underwater vehicle. *Ocean Engineering*, 181:145-160. https://doi.org/10.1016/j.oceaneng.2019.04.011

Schmidt AM, 2006. Electromagnetic activation of shape memory polymer networks containing magnetic nanoparticles. *Macromolecular Rapid Communications*, 27(14):1168-1172. https://doi.org/10.1002/marc.200600225

Shin D, Sardellitti I, Khatib O, 2008. A hybrid actuation approach for human-friendly robot design. IEEE International Conference on Robotics and Automation, p.1747-1752. https://doi.org/10.1109/ROBOT.2008.4543453

Song SH, Kim MS, Rodrigue H, et al., 2016. Turtle mimetic soft robot with two swimming gaits. *Bioinspiration & Biomimetics*, 11(3):036010. https://doi.org/10.1088/1748-3190/11/3/036010

Song Y, He B, Liu P, 2021. Real-time object detection for AUVs using self-cascaded convolutional neural networks. *IEEE Journal of Oceanic Engineering*, 46(1):56-67. https://doi.org/10.1109/JOE.2019.2950974

Stokes AA, Shepherd RF, Morin SA, et al., 2014. A hybrid combining hard and soft robots. *Soft Robotics*, 1(1):70-74. https://doi.org/10.1089/soro.2013.0002

Tolley MT, Shepherd RF, Mosadegh B, et al., 2014a. A resilient, untethered soft robot. *Soft Robotics*, 1(3):213-223. https://doi.org/10.1089/soro.2014.0008

Tolley MT, Shepherd RF, Karpelson M, et al., 2014b. An untethered jumping soft robot. IEEE/RSJ International Conference on Intelligent Robots and Systems, p.561-566. https://doi.org/10.1109/IROS.2014.6942615

Tone T, Suzuki K, 2018. An automated liquid manipulation by using a ferrofluid-based robotic sheet. *IEEE Robotics and Automation Letters*, 3(4):2814-2821. https://doi.org/10.1109/LRA.2018.2842251

Wang HP, Yang Y, Lin GZ, et al., 2021. Untethered, high-speed soft jumpers enabled by combustion for motions through multiphase environments. *Smart Materials and Structures*, 30(1):015035. https://doi.org/10.1088/1361-665X/abcaae

Wang HP, Yang Y, Ye XH, et al., 2023. Combustion-enabled underwater vehicles (CUVs) in dynamic fluid environment. *Journal of Field Robotics*, in press. https://doi.org/10.1002/rob.22167

Xin B, Luo XH, Shi ZC, et al., 2013. A vectored water jet propulsion method for autonomous underwater vehicles. *Ocean Engineering*, 74:133-140. https://doi.org/10.1016/j.oceaneng.2013.10.003

Yang Y, Hou BZ, Chen JY, et al., 2020. High-speed soft actuators based on combustion-enabled transient driving method (TDM). *Extreme Mechanics Letters*, 37:100731. https://doi.org/10.1016/j.eml.2020.100731

Yang Y, He ZG, Lin GZ, et al., 2022. Large deformation mechanics of the thrust performances generated by combustion-enabled soft actuators. *International Journal of Mechanical Sciences*, 229:107513. https://doi.org/10.1016/j.ijmecsci.2022.107513

Yao P, Zhao SQ, 2018. Three-dimensional path planning for AUV based on interfered fluid dynamical system under ocean current (June 2018). *IEEE Access*, 6:42904-42916. https://doi.org/10.1109/ACCESS.2018.2861468

Yue CF, Guo SX, Li MX, 2013. ANSYS FLUENT-based modeling and hydrodynamic analysis for a spherical underwater robot. IEEE International Conference on Mechatronics and Automation, p.1577-1581. https://doi.org/10.1109/ICMA.2013.6618149

Zhang BY, Fan YW, Yang PH, et al., 2019. Worm-like soft robot for complicated tubular environments. *Soft Robotics*, 6(3): 399-413. https://doi.org/10.1089/soro.2018.0088

Zhang LC, Huang Q, Cai KJ, et al., 2020. A wearable soft knee exoskeleton using vacuum-actuated rotary actuator. *IEEE Access*, 8:61311-61326. https://doi.org/10.1109/ACCESS.2020.2983790

Zhang SW, Liang X, Xu LC, et al., 2013. Initial development of a novel amphibious robot with transformable fin-leg composite propulsion mechanisms. *Journal of Bionic Engineering*, 10(4):434-445. https://doi.org/10.1016/S1672-6529(13)60247-4

Zhang TS, Yang L, Yang X, et al., 2021. Millimeter-scale soft continuum robots for large-angle and high-precision manipulation by hybrid actuation. *Advanced Intelligent Systems*, 3(2):2000189. https://doi.org/10.1002/aisy.202000189

Zhou F, Gu LY, Luo GS, et al., 2013. Development of a hydraulic propulsion system controlled by proportional pressure valves for the 4500m work-class ROV. OCEANS-San Diego, p.1-6. https://doi.org/10.23919/OCEANS.2013.6741049

Zi B, Yin GC, Zhang D, 2016. Design and optimization of a hybrid-driven waist rehabilitation robot. *Sensors*, 16(12): 2121. https://doi.org/10.3390/s16122121

Electronic supplementary materials

Videos S1–S6